Supplementary Information for "Homogeneous freezing of water droplets for different volumes and cooling rates" by Nadia Shardt[1*], Florin N. Isenrich[2*], Benedikt Waser[2], Claudia Marcolli[1], Zamin A. Kanji[1], Andrew J. deMello[2], Ulrike Lohmann[1]

[1]Institute for Atmospheric and Climate Science, ETH Zurich, Zürich, 8092, Switzerland
[2]Institute for Chemical and Bioengineering, ETH Zurich, Zürich, 8093, Switzerland

Correspondence: Nadia Shardt (nadia.shardt@env.ethz.ch) and Claudia Marcolli (claudia.marcolli@env.ethz.ch)

Contents

A. Droplet generation details

The microfluidic device for generating 100 µm droplets was based on that used to produce 75 µm diameter droplets reported in Isenrich et al. (2022) This new design contained two channel heights to enable droplet generation with a wider orifice of 50 µm, as illustrated in **Fig. A1**. In the employed wafer, droplet generation channels (outlined by thin, light lines) had a height of 48 µm to allow droplet generation at flowrates comparable to those used for generating 75 µm droplets. The subsequent channels (outlined by thick, dark lines) had a height of 110 µm to ensure that droplets would be spherical in the imaging window.

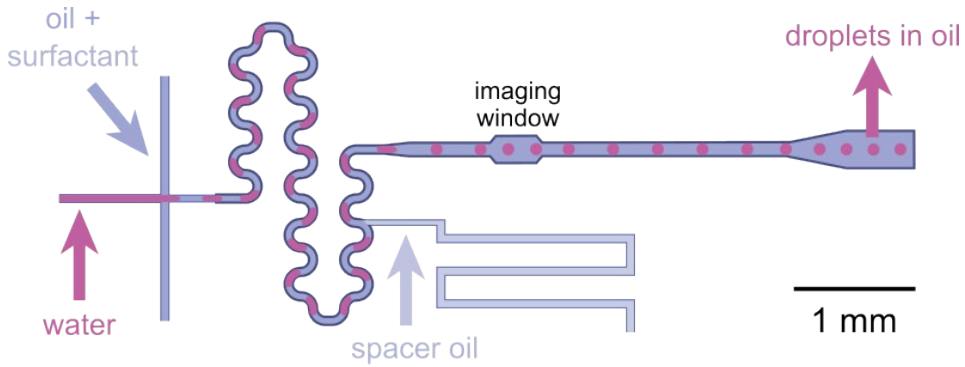

Fig. A1. Design of the microfluidic chip used to produce droplets with 100 µm diameters. Channels outlined by thin, light lines have a height of 48 µm, and channels outlined in thick, dark lines have a height of 110 µm.

Table A1 summarizes the flow rates of water, surfactant in oil, and spacer oil used to generate each population of droplets, labelled according to the target droplet diameter and the name of the experiment in **Fig. 1**. Also listed is the mean droplet diameter of each droplet population with a measurement uncertainty of ± 5 µm (due to the optics and camera resolution) and the cooling rates that each droplet population underwent.

Table A1. Flow rates of water, surfactant in oil, and spacer oil for each droplet population, along with its mean diameter and the rate at which it was cooled. The uncertainty in measuring droplet radius is estimated to be that of two pixels, which corresponds to an uncertainty in diameter of 5 μm. An asterisk (*) on the experiment name indicates that these runs were obtained by Isenrich et al. (2022) and are included here for completeness.

experiment name	Q_{water} [μL min^{-1}]	$Q_{surfactant}$ [μL min^{-1}]	$Q_{spacer\ oil}$ [μL min^{-1}]	d_{mean} [μm]	−dT/dt [K min^{-1}]
75-i and r-i	1.0	1.5	2.3	75	0.1 and 1
75-ii and r-ii	1.0	1.5	2.3	75	0.1 and 1
75-iii and r-iii	1.0	1.5	2.3	78	0.1 and 1
75-a*	1.0	1.5	2.0	75	1
75-b*	1.0	1.5	2.3	75	1
75-c*	1.0	2.0	1.4	78	1
100-i and r-i	2.3	2.0	4.0	103	0.1 and 1
100-ii and r-ii	2.3	2.0	4.0	100	0.1 and 1
100-iii and r-iii	2.3	2.0	4.0	98	0.1 and 1
100-a	2.0	2.0	3.7	98	1
100-b	2.0	2.0	3.7	98	1
100-c	2.3	2.0	4.0	98	1

B. Spatial distribution of freezing events and cooling rate for each experiment

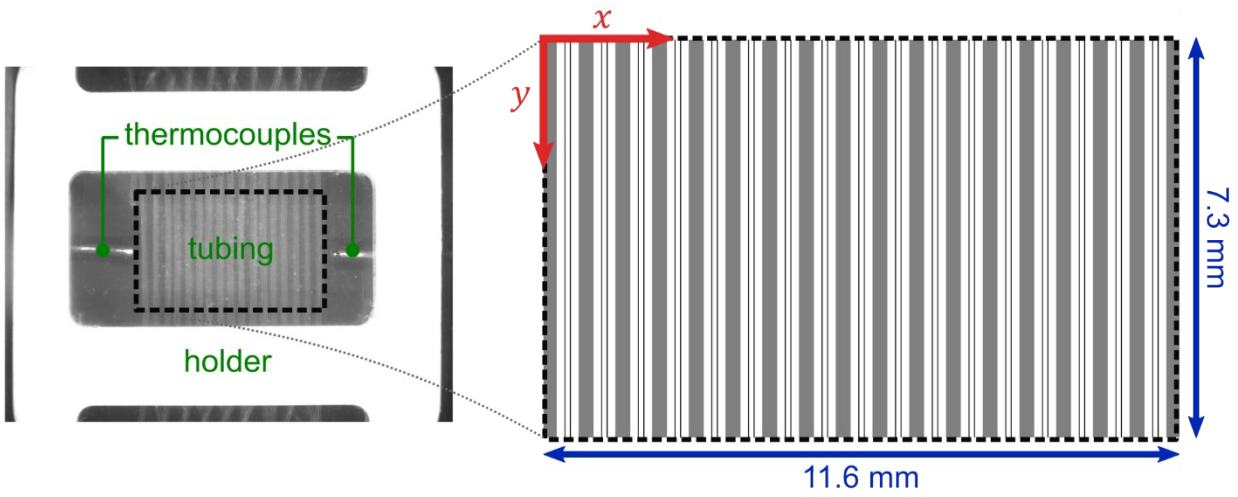

Fig. B1. Schematic of the PFA tubing that contains droplets seen from a top-down view by the camera. The aluminium bath in the background is shaded in grey. For illustrative purposes, we define *x*- and *y*-axes to orient the reader when interpreting droplet locations in **Figs. B2–B4**.

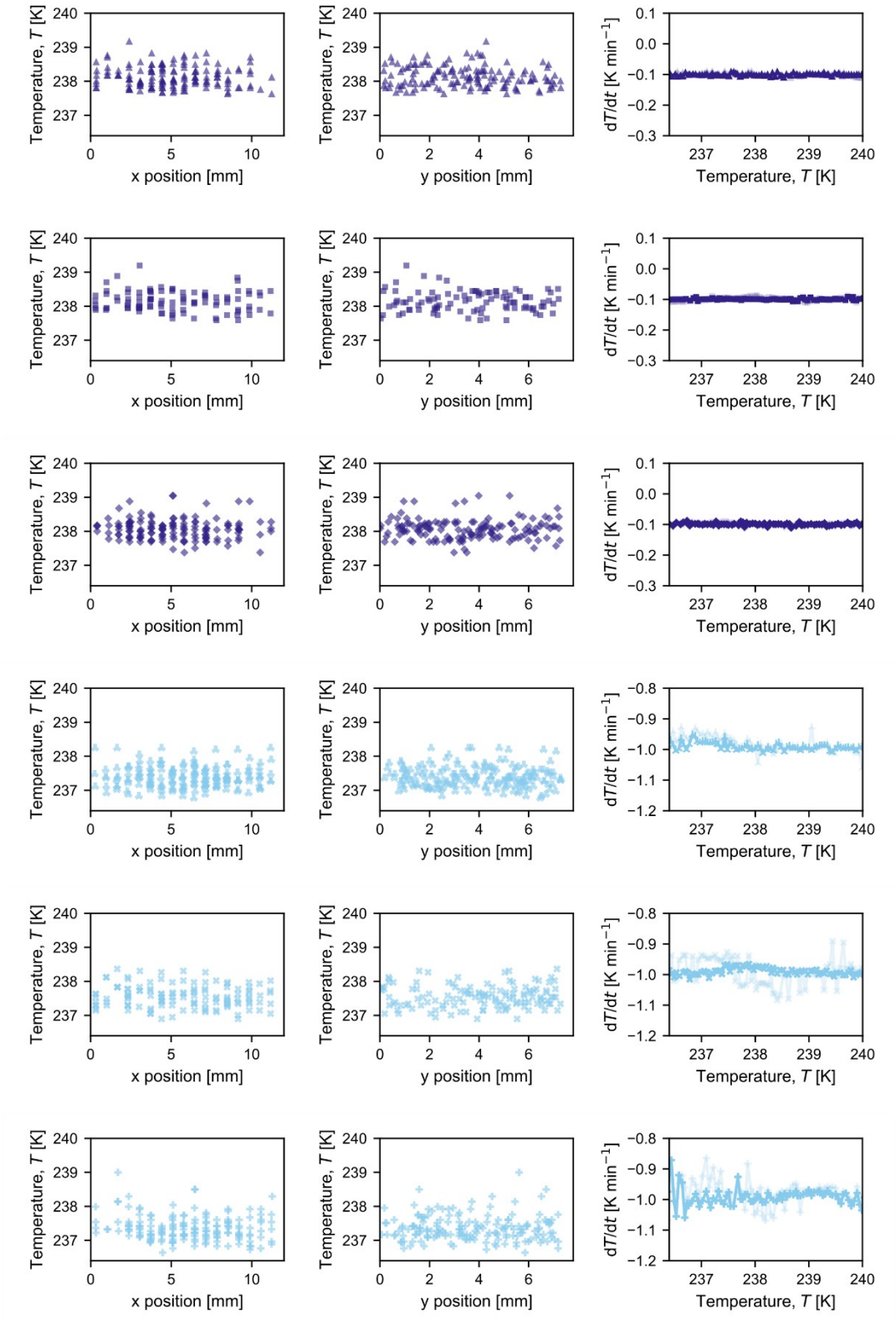

Fig. B2. Observed freezing temperature at each *x* and *y* position (see schematic in Figure B1) for experiments on 75 µm droplets shown in Figure 1a cooled at 0.1 K min^{-1} (top three rows) and refrozen at 1 K min^{-1} (bottom three rows). The third graph in each row shows the measured cooling rate at each temperature where a picture was taken. The opaque line indicates the cooling rate measured by the thermocouple that was used as input to the control loop, and the semi-opaque line indicates the cooling rate measured by the second thermocouple in the bath.

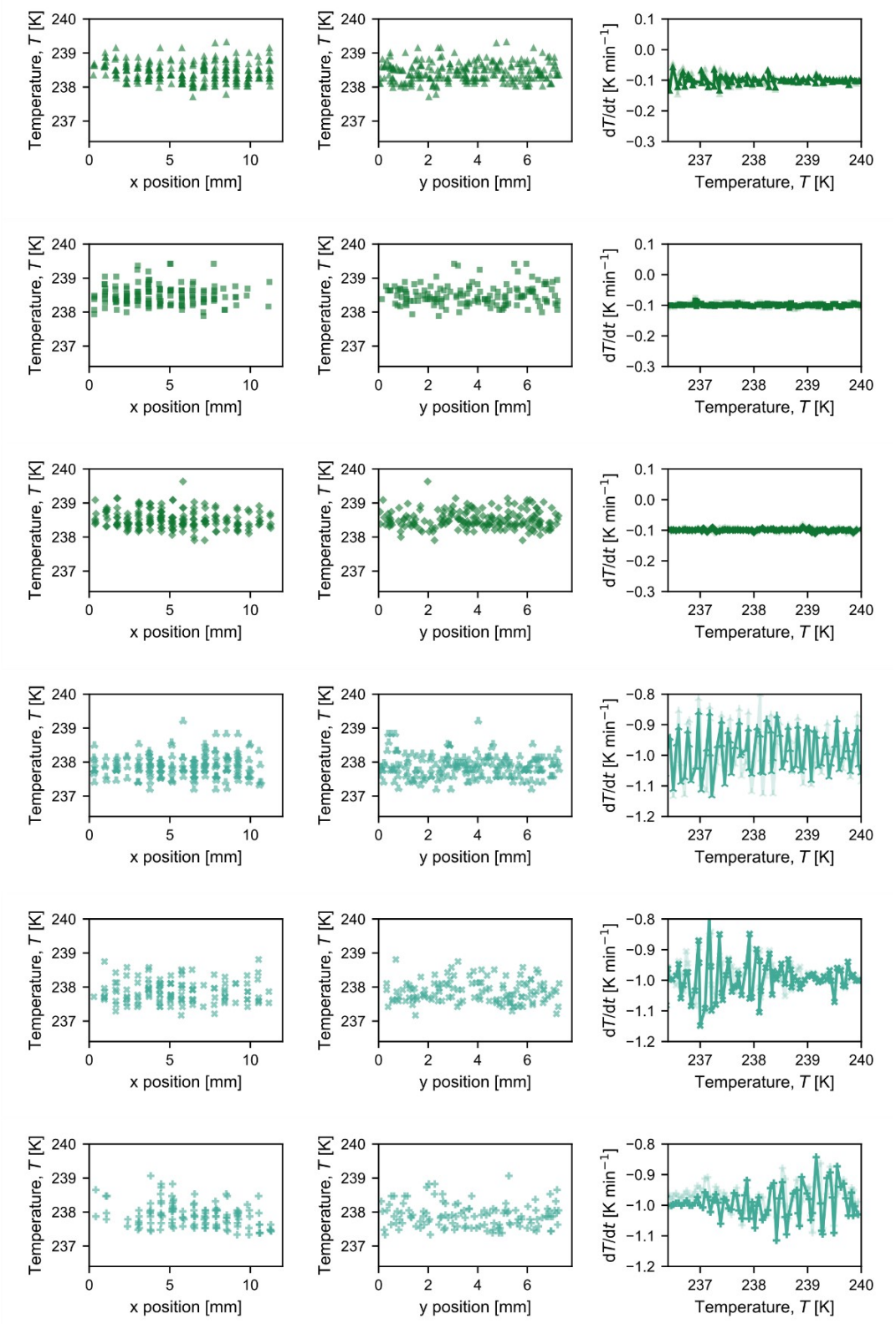

Fig. B3. Observed freezing temperature at each x and y position (see schematic in Figure B1) for experiments on 100 µm droplets shown in Figure 1b cooled at 0.1 K min^{-1} (top three rows) and refrozen at 1 K min^{-1} (bottom three rows). The third graph in each row shows the measured cooling rate at each temperature where a picture was taken. The opaque line indicates the cooling rate measured by the thermocouple that was used as input to the control loop, and the semi-opaque line indicates the cooling rate measured by the second thermocouple in the bath.

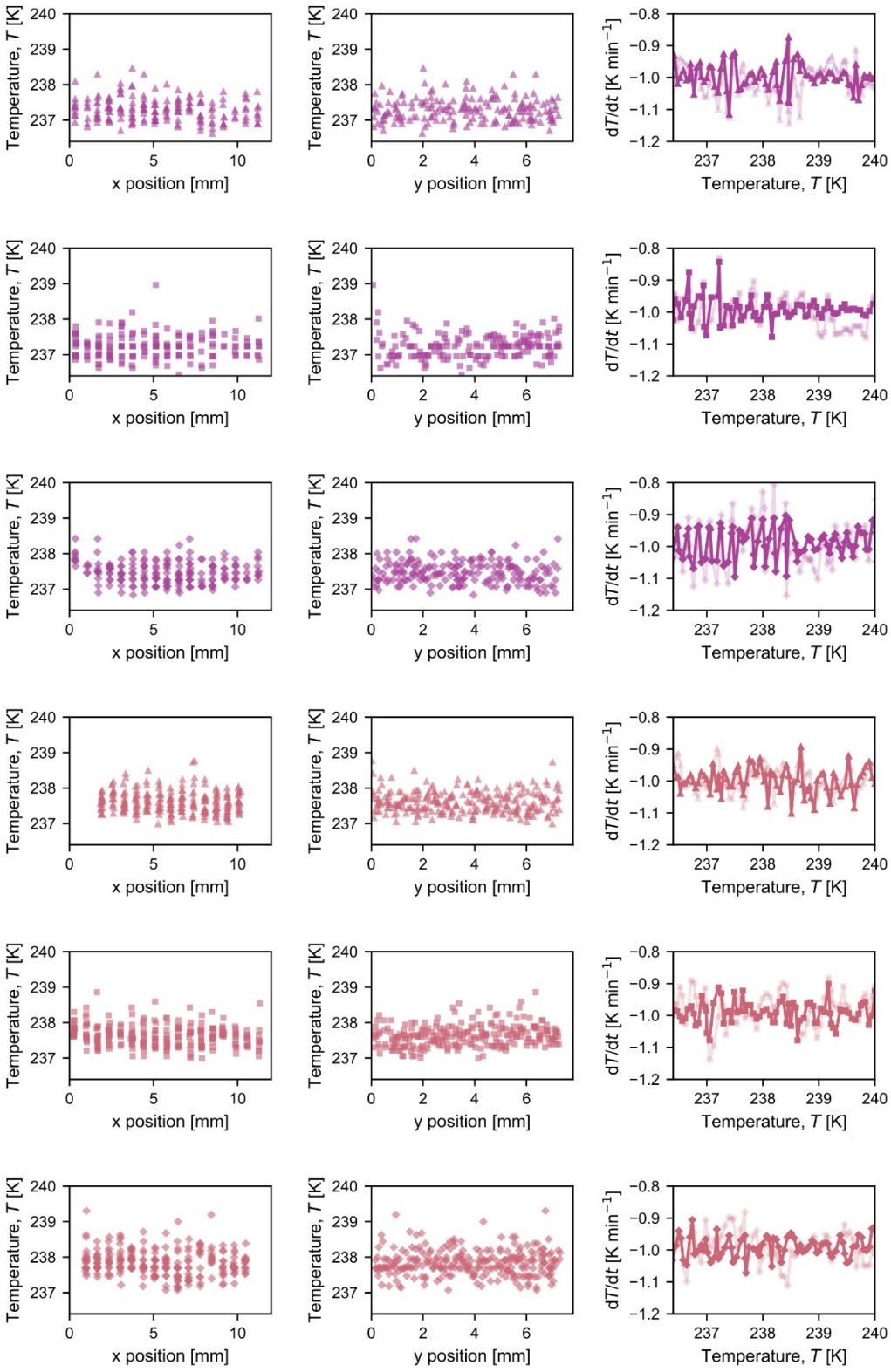

Fig. B4. Observed freezing temperature at each x and y position (see schematic in Figure B1) for experiments on 75 µm (top three rows) and 100 µm droplets (bottom three rows) shown in Figure 1 cooled at 1 K min^{-1}. The third graph in each row shows the measured cooling rate at each temperature where a picture was taken. For completeness, the top three rows corresponding to 75 µm droplets are reproduced from the Appendix in the work of Isenrich et al. (2022) The opaque line indicates the cooling rate measured by the thermocouple that was used as input to the control loop, and the semi-opaque line indicates the cooling rate measured by the second thermocouple in the bath.

C. Ickes et al. (2015) parameterisation (I15) details

The parameterisation given by Ickes et al. (2015) is based on classical nucleation theory and has the form:

$$J_{hom} = C\exp\left(-\frac{\Delta g^{\#}}{k_B T}\right)\exp\left(-\frac{\Delta G}{k_B T}\right) \quad \text{(C1)}$$

where $C = 10^{35}\ cm^{-3}\ s^{-1}$, k_B is the Boltzmann constant, T is temperature, $\Delta g^{\#}$ is the diffusional activation energy, and ΔG is the thermodynamic energy barrier, which are calculated as follows (Zobrist et al., 2007):

$$\Delta g^{\#} = \frac{892\ K\ k_B T^2}{(T - 118\ K)^2} \quad \text{(C2)}$$

$$\Delta G = \frac{16\pi\, v_{ice}^2(T)\sigma_{sl}^3(T)}{3\ \left(k_B T \ln S(T)\right)^2} \quad \text{(C3)}$$

where the molecular volume of ice v_{ice} and the saturation ratio S (ratio between the equilibrium vapour pressure of supercooled liquid and that of ice) depend on temperature using the parameterisations outlined in Zobrist et al. (2007) and Murphy and Koop (2005) for hexagonal ice. The solid–liquid interfacial tension σ_{sl} is calculated using the parameterisation from Reinhardt and Doye (2013):

$$\sigma_{sl}\,[J \cdot cm^{-2}] = 3 \times 10^{-6} - 1.8 \times 10^{-8}(273.15 - T) \quad \text{(C4)}$$

D. Monte Carlo simulations for distributions of droplet volume and cooling rate

To investigate the effect of variations in droplet volume on the observed nucleation rates, we sample droplet diameters from a Gaussian distribution with a mean droplet diameter of either 75 or 100 µm and a standard deviation of 5 µm. We perform simulations using the same conditions as investigated experimentally, including the number of droplets, cooling rates, and number of experiments. **Fig. C1**a shows nucleation rates as a function of temperature when calculated based on individual frozen fractions, while the nucleation rates in **Fig. C1**b are determined based on the merged frozen fraction for each mean droplet diameter and cooling rate. Then, we sample cooling rates from a Gaussian distribution with a mean of either 0.1 or 1 K min^{-1} and a standard deviation of 10 %, shown in **Fig. C1**c–d (individual vs merged frozen fractions, respectively). Finally, we consider a simulation where both droplet diameter and cooling rate are sampled from Gaussian distributions, shown in **Fig. C1**e–f.

A standard deviation of 5 µm in droplet diameter has a greater impact on the number of droplets that freeze at warmer temperatures than a standard deviation of 10 % in cooling rate. In all simulations, considering individual frozen fractions (**Fig. C1**a, c, and e) results in a significant variation of the calculated nucleation rates around the underlying nucleation rate (the parameterisation from Ickes et al. (2015)). By combining the frozen fractions from simulations completed at the same droplet diameter

and cooling rate, the scatter in the calculated nucleation rates is significantly reduced. Overall, therefore, the total number of droplets considered in a single frozen fraction has a larger impact on the calculated nucleation rate than variations in either droplet diameter or cooling rate (i.e., the vast majority of nucleation rates in panels (b), (d), and (f) are similarly dispersed around the underlying nucleation rate no matter the variation in droplet diameter and cooling rate).

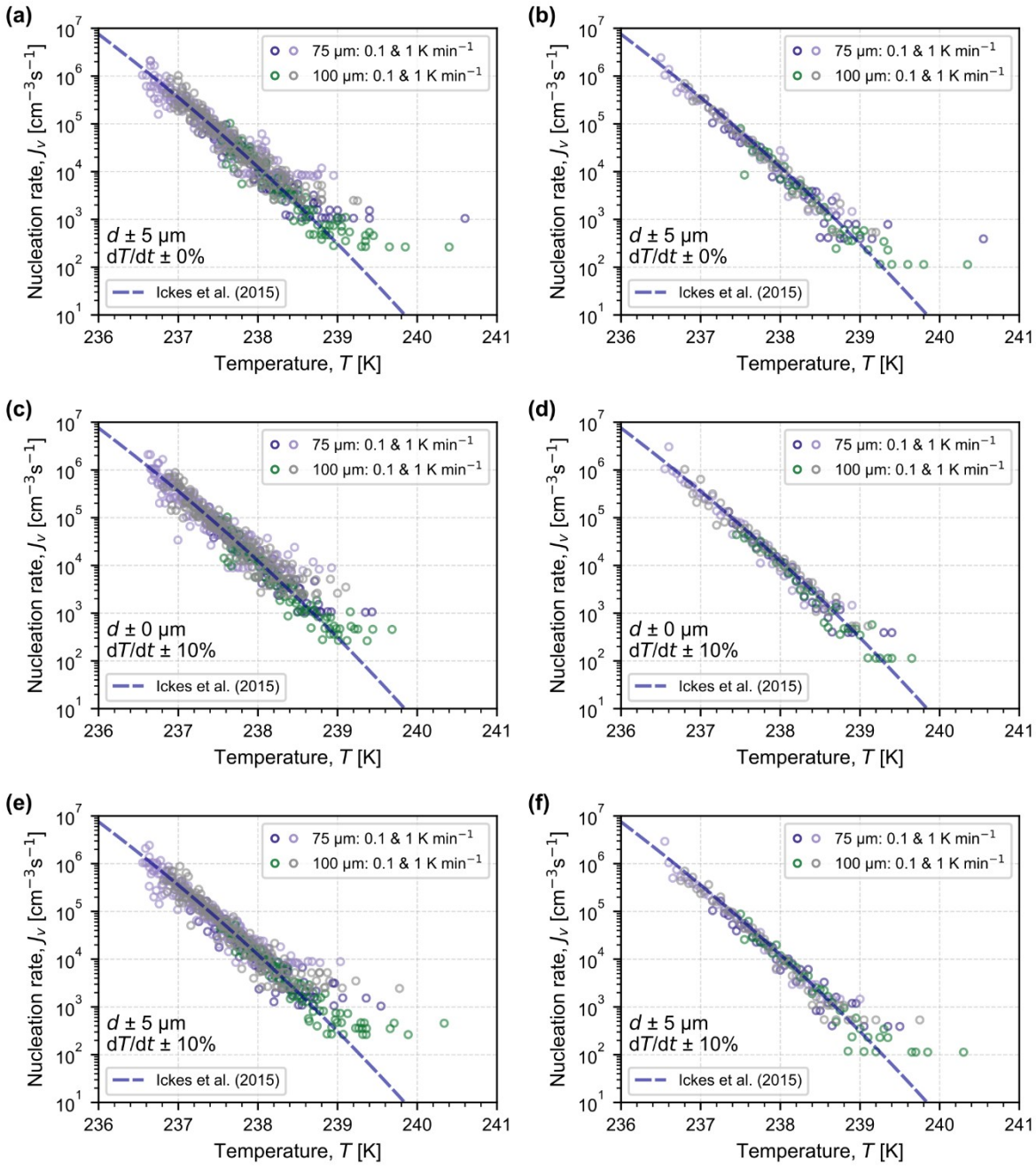

Fig. D1. Nucleation rates calculated from Monte Carlo simulations of droplets freezing with (a–b) a Gaussian distribution of droplet diameter with a standard deviation of 5 µm, calculated based on (a) individual frozen fractions and based on (b) the merged frozen fractions; (c–d) a Gaussian distribution of cooling rate with a standard deviation of 10 %, calculated based on (c) individual frozen fractions and based on (d) the merged frozen fractions; (e–f) Gaussian distributions for both droplet diameter and cooling rate, calculated based on (e) individual frozen fractions and based on (f) the merged frozen fractions.

References

Ickes, L., Welti, A., Hoose, C. and Lohmann, U.: Classical nucleation theory of homogeneous freezing of water: Thermodynamic and kinetic parameters, Phys. Chem. Chem. Phys., 17(8), 5514–5537, doi:10.1039/c4cp04184d, 2015.

Isenrich, F. N., Shardt, N., Rösch, M., Nette, J., Stavrakis, S., Marcolli, C., Kanji, Z. A., DeMello, A. J. and Lohmann, U.: The Microfluidic Ice Nuclei Counter Zürich (MINCZ): A platform for homogeneous and heterogeneous ice nucleation, Atmos. Meas. Tech. Discuss., 1–24, 2022.

Murphy, D. M. and Koop, T.: Review of the vapour pressures of ice and supercooled water for atmospheric applications, Q. J. R. Meteorol. Soc., 131(608), 1539–1565, doi:10.1256/qj.04.94, 2005.

Reinhardt, A. and Doye, J. P. K.: Note: Homogeneous TIP4P/2005 ice nucleation at low supercooling, J. Chem. Phys., 139(9), 096102, doi:10.1063/1.4819898, 2013.

Zobrist, B., Koop, T., Luo, B. P., Marcolli, C. and Peter, T.: Heterogeneous ice nucleation rate coefficient of water droplets coated by a nonadecanol monolayer, J. Phys. Chem. C, 111(5), 2149–2155, doi:10.1021/jp066080w, 2007.